RP Current Trends In Applied Sciences (e-ISSN: 2583-7486)
Vol. 4, No. 3 (July – September 2025) pp. 31–45

RESEARCH PLATEAU PUBLISHERS

Cite this article: Pravesh, Quantum corrections on optical phase conjugation via stimulated Brillouin scattering in ion-implanted semiconductor plasmas, *RP Cur. Tr. Appl. Sci.* **4** (2025) 31–45.

Original Research Article

Quantum corrections on optical phase conjugation via stimulated Brillouin scattering in ion-implanted semiconductor-plasmas

Pravesh*

Department of Physics, Baba Mastnath University, Asthal Bohar, Rohtak – 124021, Haryana, India
*Corresponding author, E-mail: praveshlamba004@gmail.com

ARTICLE HISTORY
Received: 8 April 2025
Revised: 8 July 2025
Accepted: 12 July 2025
Published: 14 July 2025

KEYWORDS
Quantum effects; Optical phase conjugate mode; Ion-implantation; Stimulated Brillouin scattering (SBS); Brillouin susceptibility; Quantum hydrodynamic model; Threshold pump intensity; Reflectivity enhancement.

ABSTRACT
Quantum effects (QEs) on the threshold and reflectivity characteristics of the optical phase conjugate mode (OPCM) in ion-implanted semiconductor plasmas are analytically investigated using coupled mode theory. Taking into account that the origin of stimulated Brillouin scattering lies in nonlinear induced polarisation of the medium, expressions are derived for complex effective Brillouin susceptibility (due to electrons and implanted colloids) and consequently the threshold pump intensity and the reflectivity of OPCM. Inclusion of QEs is done via quantum correction term in the hydrodynamic model of semiconductor plasmas. QEs modify the threshold and the reflectivity characteristics of OPCM in ion implanted semiconductor plasmas. Finally, an extensive numerical study of the n- InSb/CO_2 laser system is performed for two different cases: (i) without QEs and (ii) with QEs. In both cases, the analysis offers two achievable resonances, at which an enhancement of reflectivity of OPCM is obtained at excitation intensities well below the optical damage threshold if ion-implanted semiconductor-plasma is used as an optical waveguide with an interaction length of a few millimetres. When QEs are included in the analysis, the entire spectrum shifts towards decreased levels of electron and colloidal carrier concentration. The results suggest that a high reflectivity optical phase conjugate mirror can be fabricated using n-InSb-CO_2 system as the outcome of this research work.

1. Introduction

Optical phase conjugation (OPC) is a nonlinear optical phenomenon observed since 1970's [1]. Since this phenomenon is realistic for use in various important applications ranging from optical signal processing, image transmission, laser resonators, high-brightness laser systems, filtering and ultra-low noise communication schemes [2-6], the investigation of OPC has become an active field of research in the area of quantum optics.

Among the various existing techniques of OPC, the most promising are: three-wave mixing (TWM) and four-wave mixing (FWM) [7, 8] and stimulated scatterings processes [9]. In OPC studies, a large number (many thousands) of research articles have been published since 1970's. Many of them are based on the technique of degenerate four-wave mixing (DFWM) in various nonlinear optical media with minor theoretical modifications. In the present research work, SBS technique is employed to study OPC in ion-implanted semiconductor plasmas [10].

Before proceeding further, it is essential to understand the physics behind OPC-SBS. An intense pump wave $\vec{E}_0(\omega_0,\vec{k}_0)$ illuminates the Brillouin active medium. The wave is passed through an external distorting medium, which makes the intensity distribution of the pump in the nonlinear medium both in the longitudinal and transverse coordinates and thereafter the distorted pump wave interacts with the Brillouin active medium. The Stokes wave $\vec{E}_s(\omega_s,\vec{k}_s)$ develops from the spontaneous noise in a direction opposite to the direction of incident pump wave and is exponentially amplified due to SBS process as it travels in backward direction towards the entrance window of the cell containing the SBS medium. The amplified Stokes wave contains a transverse structure which is phase conjugate of the pump wave, known as optical phase conjugate mode (OPCM).

First of all, the research group of Zel'dovich et al. [1], while illuminating a CH_4 gas multimode waveguide by a ruby laser, observed the important phenomenon of OPC-SBS. They found that the scattering efficiency decreases exponentially at low laser power. It was suggested that efficient scattering can be obtained at low laser power without using the feedback to enhance the interaction [11]. OPC-SBS with incorporating optical feedback was experimentally demonstrated and studied analytically to lower the threshold value of pump intensity and enhance the reflectivity of OPCM [12]. This technique makes use of number of beam splitters. OPC technique minimizes the phase distortions encountered by aberrations arising when a coherent wave travels through an imperfect medium. In OPC technique, the aberrations get subtracted from the distorted coherent wave when a phase conjugate wave is allowed to pass back through the nonlinear medium. Zel'dovich et al. [13] suggested that the phenomenon of OPC-SBS have its origin in the backscattered component of coherent wave having frequency down/up shift equal to the acoustical phonon frequency. This component varies exponentially as faster as double the rate of variation of other modes. Under the regimes

of high-gain, this backscattered component dominates over other random modes and the reflectivity of OPCM even approaches 100%. Using this technique, high reflectivity of OPCM may be obtained. Thus, under regimes of high gain, an aberrated pump wave supports the amplification of a single (optical phase conjugate) mode.

OPC-SBS can be established in a Brillouin active medium at excitation intensity greater than the threshold intensity. Anderson et.al. [14] reported that OPC signals of 4×10^{-17} J/pulse can be obtained by inserting an input pre-amplifier. Ridley and Scott [15] obtained OPC signals of 3×10^{-13} J/pulse by introducing an amplifier of high gain in the geometry of OPC-SBS. They observed that the use of pre-amplifier into the geometry of OPC-SBS significantly reduces the threshold value of pump intensity required for the process of OPC-SBS. Hellwarth [16] reported that the fidelity of OPCM in a waveguide structure is a function of pump energy distribution among various modes of vibration and is independent of the excitation intensity. Suni and Falk [17] assigned the origin of this discrepancy to a different treatment of phase mismatched scattering terms. The theoretical results discussed above do not incorporate the pump depletion, which becomes pre-dominant at pump intensities well above the threshold intensity of OPCM. Lehmberg [18] reported that in OPC-SBS waveguide structures, the pump depletion increases the fidelity by retarding the small-scale pulling effect. Scott and Hazell [19] on the basis of theoretical formulations developed for transient state All the theoretical results discussed above were formulated on OPC-SBS by looking its applications in optical fiber communication. However, the phenomenon of OPC-SBS in a Brillouin cell, consisting of III-V semiconductors, could have a great potential in obtaining enhanced reflectivity of OPCM, which has potential applications in laser-plasma induced fusion.

The doped semiconductors such as n-InAs, n-GaAs, n-InSb etc. are the host materials which exhibit Brillouin nonlinearity (χ_B) [20]. This is due to the excess of free carriers in these media [21]. Moreover, χ_B can be significantly enhanced by the application of an external magnetic field [21]. Aghamkar and Singh [22] studies OPC-SBS in weakly piezoelectric magnetized semiconductor plasmas. Singh and Aghamkar [22] studies OPC-SBS in narrow bandgap semiconductors. Singh et al. [23] studies OPC-SBS in magnetized diffusion driven semiconductors. Bhan et al. [24] studied the threshold and reflectivity characteristics of OPCM in transversely magnetized semiconductors. Apart from this, χ_B may be affected by implanted colloids concentration in ion-implanted semiconductor plasmas (IISPs).

The fabrication of semiconductor plasmas with regulated impurity profiles frequently uses the doping technique of ion implantation. However, because the implantation procedure damages the crystal lattice, post-implantation annealing is required to restore the lattice to a high degree and activate the dopants electrically [25]. The structural, electric, magnetic, (linear and nonlinear) optical properties of semiconductors can be modified by the implanted ions [26]. As a result, its primary use is in the development of semiconductor components. The depth profile of the implanted ion may be explained by chemical binding effects linked to ion-ion and ion-target atom interactions at low energies [27]. As a result of this process, the implanted metal ions are neutralised during the slowing processes and eventually agglomerate to produce colloids of implanted materials.

The host material would display a variety of valuable thermodynamic, electrical, and optical properties that can be easily controlled, though, if the colloid particles could somehow be aligned in a long-range periodic fashion. Ion implantation is a popular method for creating diverse nanofabrication tools. The formation of tiny colloid particles in a long-range order lattice in magnetized and inhomogeneous semiconductor quantum plasmas has been studied theoretically [28, 29]. A stream of electrons with a drift speed similar to the ion-acoustic phonon speed in the crystal may be driven by the presence of an external drift field considerably below the breakdown of the semiconductor. By causing consistent electron current, these external fields can charge the growing colloid particles by sticky collisions. By using this method, colloidal plasma will be created, which resembles dusty plasma in that it contains electrons, negatively charged colloid particles, and vibrating positive lattice ion centres. This medium will become an IISP medium. In-depth research [30, 31] has been done on the function of charged colloids in IISPs for both identifying new modes of propagation and amplifying the waves of already existing modes. The existence of numerous novel modes and creative alterations to the characteristics of already-existing modes of propagation in IISPs has been demonstrated [32]. The most recent results further show that, even at frequencies where colloidal grains do not contribute to the linear motion of waves, the presence of charged colloids in IISPs has a significant impact on the wave properties of existing modes [33]. The colloids in these situations offer an immovable charge-neutralizing backdrop in IISPs.

Researchers have been concentrating their efforts on theoretical investigations of quantum effects (QEs) in plasmas for a long time. In super cooled plasmas, the de-Broglie wavelength connected to plasma particles approaches the Debye length [34]. It is possible to extend the magneto-hydrodynamic model of classical plasmas to encompass quantum plasmas; this newly created model is referred to as the quantum hydrodynamic (QHD) model [35]. In its most basic form, the QHD model is the generalisation of the classical hydrodynamic (CHD) model of plasmas with the inclusion of the quantum (Bohm potential) correction factor. Recently, this approach has been applied to the analytical study of QEs on parametric interactions [36], modulational interactions [37, 38], and SBS [39] in semiconductor magneto-plasmas.

For relatively large density of implanted colloids, QEs could become highly important in IISPs. The formation of colloid crystals in IISP has been reported by Zeba et al. [29]. Through the use of the Bohm potential, they have demonstrated that QEs on lattice electron-phonon coupling effects contribute to the dielectric response function of IISP. My research group has recently investigated QEs on modulational amplification characteristics [40] and Brillouin amplification characteristics of SBS [41] in IISPs. In these investigations, we found that including QEs reduced the threshold pump amplitude for the onset of modulational and Brillouin amplification and enhances the growth rate of the

modulated beam and Brillouin gain coefficient for both the electrons and implanted colloids.

According to a literature review, QEs have not been investigated on OPC-SBS in IISPs. In the present chapter, we conduct a theoretical formulation followed by a numerical analysis to examine the threshold and reflectivity characteristics of OPCM in IISPs under two different cases of interest, namely (i) the inclusion of QEs and (ii) the exclusion of QEs, keeping in mind the significant impact of QEs on OPC-SBS in IISPs. Expressions for the complex effective Brillouin susceptibility (caused by electrons and implanted colloids) are obtained using coupled mode theory of interacting waves and the assumption that the origin of OPC-SBS lies in finite nonlinear induced polarisation and consequently the complex effective Brillouin susceptibility of IISPs. The complex effective Brillouin susceptibility is used to calculate the threshold intensity and reflectivity of OPCM. In order to enhance the reflectivity of OPCM at low pump intensities, efforts are made to optimise the concentration of electrons and implanted colloids as well as to set the value of the electron-plasma frequency and dust plasma frequency. Finally, an extensive numerical study is performed for n-InSb irradiated by a pulsed CO_2 laser.

The fact that implanted colloids, in addition to electrons, may significantly alter Brillouin nonlinearity and, as a result, the propagation characteristics of OPCM in IISPs, serves as the impetus for this investigation. This investigation becomes even more essential under high power pump irradiation since it helps to better understand OPC-SBS in IISPs. The threshold and reflectivity characteristics of OPCM in IISPs have been modified in comparison to earlier studies of OPC-SBS in semiconductor magneto-plasmas using the CHD model [24], which makes this work a novel study with applications in the development of efficient phase conjugate mirrors.

2. Effective Brillouin susceptibility

In this section, an expression is obtained for the effective Brillouin susceptibility (including QEs) in IISPs. For this, CHD model of homogeneous one-component semiconductor magneto-plasma (i.e. $k_a l \ll 1$, where k_a is the acoustic phonon mode number and l the carrier mean free path) has been extended to take account of quantum corrections resulting into one-component semiconductor quantum plasma depicted by subsequent QHD model.

In IISPs, SBS occurs due to nonlinear interaction among three coherent fields, viz.

(i) an intense pump field $E_0(x,t) = E_0 \exp[i(k_0 x - \omega_0 t)]$,

(ii) an induced acoustic phonon mode $u(x,t) = u_0 \exp[i(k_a x - \omega_a t)]$, and

(iii) a scattered Stokes component of pump field $E_s(x,t) = E_s \exp[i(k_s x - \omega_s t)]$.

Here $(\omega_0, \vec{k}_0)$, $(\omega_a, \vec{k}_a)$, and $(\omega_s, \vec{k}_s)$ represent the pump wave, acoustic phonon, and Stokes wave frequencies and wave number's, respectively.

The set of hydrodynamic (usually momentum transfer and continuity) equations that contain QEs via the Bohm-like potential are used to describe the carrier dynamics. Purely QEs are introduced by quantum statistics and the novel force associated with the quantum Bohm potential. Instead of dealing with the complexity of the Schrodinger-Poisson (2N equations), the QHD model is a simplified model that enables uncomplicated examination of the collective dynamics.

If IISP contains negatively charged colloids, the following is the requirement for charge neutrality:

$$n_{0i} = Z_{0d} n_{0d} + n_{0e}. \tag{1}$$

The number of unaffected charges that are present on the colloid grain is given by the symbol Z_{0d} (expressed in units of electronic charge). n_{0d}, n_{0e} and n_{0i} are the carrier densities of colloid grain, electrons, and unperturbed ions, respectively. The ultra-cold IISP acts like a Fermi gas and abides by the pressure law because, as IISP cools, the plasma carriers' de-Broglie wavelengths become equivalent to the system dimensions [35]. Equation (2), which has been modified partly to take into account the Fermionic property of the colloids, is used in the model to incorporate quantum statistics.

$$P_{Fl} = \frac{m_l V_{Fl}^2 n_{1l}^3}{3 n_{0l}^2}, \tag{2}$$

In equation (2), P_{Fl} is the Fermi pressure, where the subscript l = e, d stand for electrons and implanted colloids, respectively. n_{0l} and n_{1l} are unperturbed and perturbed electron densities, respectively. m_l is the mass of plasma carriers. $V_F (= 2k_B T_F / m)$ represents the Fermi speed, in which T_F is the Fermi temperature and k_B is the Boltzmann constant. The interpretation of pressure is based on the fluid's mean velocity being dispersed at different rates. The pressure term selected in this case is calculated under the assumption that electrons and colloids with homogeneous grain size are characterised by a zero temperature Fermi distribution function.

In QHD model, the basic equations that describe SBS in IISP are as follows:

$$\frac{\partial^2 u(x,t)}{\partial t^2} - \frac{C}{\rho}\frac{\partial^2 u(x,t)}{\partial x^2} + 2\Gamma_a \frac{\partial u(x,t)}{\partial t} = \frac{\beta}{\rho}\frac{\partial E_1}{\partial x} \tag{3}$$

$$\frac{\partial v_{0l}}{\partial t} + \nu v_{0l} = -\frac{Z_l e}{m_l} E_0 \tag{4}$$

$$\frac{\partial v_{1l}}{\partial t} + \nu v_{1l} + \left(v_{0l} . \frac{\partial}{\partial x}\right) v_{1l} = -\frac{Z_l e}{m_l} E_s - \frac{1}{m_l n_0}\frac{\partial P}{\partial x} + \frac{\hbar^2}{4 m_l^2 n_{0l}}\frac{\partial^3 n_{1l}}{\partial x^3} \tag{5}$$

$$v_{0l}\frac{\partial n_{1l}}{\partial x}+n_{0l}\frac{\partial v_{1l}}{\partial x}=-\frac{\partial n_{1l}}{\partial t} \tag{6}$$

$$\frac{\partial E_1}{\partial x}+\frac{\beta}{\varepsilon}\frac{\partial^2 u}{\partial x^2}=-\frac{Z_l e n_{1l}}{\varepsilon}. \tag{7}$$

Equation (3) represents the generated acoustic phonon mode in an IISP. Here β is the piezoelectric constant, C is the elastic constant, ρ is the material density, Γ_a is the phenomenological damping parameter of the acoustic phonon mode, and $u(x,t)=u\exp[i(k_a x-\omega_a t)]$ is the lattice displacement. The term on right hand side of equation (3) is the driving force per unit material density having its origin in piezoelectric property of the medium. Equations (4) and (5) are the momentum balance equations impacted by pump (E_0) and scattered (E_s) fields; v_{0l} and v_{1l} are the 0th and 1st order oscillatory fluid velocities of carriers. Here $Z_l e$ is the charge and ν the momentum transfer collision frequency of carriers. The ratio of negative charges q_d present over the colloidal grains to the charge e may be used to characterise the charge state of carriers $Z_l(=q_l/e)$. Equation (6) represents the continuity equation for carriers, where n_{1l} and n_{0l} are the perturbed and equilibrium carrier densities, respectively. The Poisson's equation [Equation (7)] can be used to calculate the strong space charge field E_1 that was created as a result of charge carriers migration under the effect of the pump field. $\varepsilon=\varepsilon_0\varepsilon_1$ is the dielectric permittivity, in which ε_0 and ε_1 being the free space permittivity and lattice dielectric constant of IISP, respectively.

The carrier density perturbation that results from the interaction of the pump wave and generated acoustic phonon mode leads to the electron plasma wave (EPW) and generates nonlinear current density in IISP. The equation for this EPW is obtained by using the linearised perturbation theory [31]. Differentiating equation (6) with respect to time, substituting the first-order differential coefficient of the 0th and 1st order oscillatory fluid velocities of carriers through equations (4) and (5), space charge field through equation (7) and assuming $n_{1a}\propto\exp[i(k_a x-\omega_a t)]$ and $n_0, v_0\propto\exp[i(k_0 x-\omega_0 t)]$, we obtain

$$\frac{\partial^2 n_{1l}}{\partial t^2}+(\omega_{pl}^2+k^2V_{Fl}^{'2})n_{1l}+\nu\frac{\partial n_{1e}}{\partial t}+\frac{Z_l e n_{0l}\beta}{m_l\varepsilon}\frac{\partial^2 u}{\partial x^2}=-\bar{E}_l\frac{\partial n_{1l}}{\partial x} \tag{8}$$

with $\bar{E}_l=-\left(\frac{Z_l e}{m_l}E_0\right)$, $V_{Fl}^{'}=V_{Fl}(1+\gamma_{el})^{1/2}$,

and $\gamma_{el}=\frac{\hbar^2k^2}{8m_l k_B T_{Fl}}$

and $\omega_{pl}=\left(\frac{(Z_l)^2 n_{0l}e^2}{m_l\varepsilon}\right)^{1/2}$ (plasma frequency).

In obtaining equation (8), the Doppler shift has been disregarded under the assumption: $\omega_0 >> \nu >> kv_0$ [42].

The generation of one induced acoustic and one Brillouin scattered photon at the same time as the annihilation of one pump photon, is another way to define SBS. By this prospective, the transfer of energy among the pump, the induced acoustic, and the Brillouin scattered waves may be described by the following momentum and energy conservation relations: $\hbar k_0=\hbar k_a-\hbar k_s$ and $\hbar\omega_0=\hbar\omega_a+\hbar\omega_s$. The Brillouin shift is determined by these equations, which are also referred to as the phase matching requirements. We can only take into account the resonant Stokes component ($\omega_s=\omega_0-\omega_a$, $k_s=k_0-k_a$) and disregard the higher-order components that are off-resonant by assuming that the interacting waves have a long interaction path [43]. It is possible to distinguish between the fast (n_{fl}) and slow (n_{sl}) components of the perturbed carrier density (n_{1l}) induced in IISP, i.e. $n_{1l}=n_{fl}+n_{sl}$, where the subscript $l=e$ (for electrons) and d (for implanted colloids). Hence, we may express: $n_{1e}=n_{fe}+n_{se}$ (for electrons) and $n_{1d}=n_{fd}+n_{sd}$ (for implanted colloids), where n_{fe} and n_{se} are the fast and slow components of the perturbed electron density (n_{1e}), respectively and n_{fd} and n_{sd} are the fast and slow components of the perturbed implanted colloids density (n_{1d}), respectively. The fast component n_{fl} and hence $n_{fe}; n_{fd}(\propto\exp[i(k_s x-\omega_s t)])$ corresponds to scattered Stokes mode whereas; the slow component n_{sl} and hence $n_{se}; n_{sd}(\propto\exp[i(k_a x-\omega_a t)])$ are associated with the induced acoustic phonon mode. By resolving equation (8) into fast and slow components of perturbed carrier density, we obtain the following coupled equations:

$$\frac{\partial^2 n_{fl}}{\partial t^2}+\nu\frac{\partial n_{fe}}{\partial t}+(\omega_{pl}^2+k^2V_{Fl}^{'2})n_{fl}=-\bar{E}_l\frac{\partial n_{sl}^{*}}{\partial x} \tag{9a}$$

$$\frac{\partial^2 n_{sl}}{\partial t^2}+\nu\frac{\partial n_{se}}{\partial t}+(\omega_{pl}^2+k^2V_{Fl}^{'2})n_{sl}+\frac{Z_l e n_{0l}\beta}{m_l\varepsilon}\frac{\partial^2 u}{\partial x^2}=-\bar{E}_l\frac{\partial n_{fl}^*}{\partial x}. \quad (9b)$$

The fast and slow components of the perturbed carrier density are denoted by the subscripts *f* and *s*, respectively. Indicators with an asterisk (*) represent the quantity's complex conjugate.

Equations (9a) and (9b) demonstrate how n_{fl} and n_{sl} are connected to one another by a pump electric field E_0 (via $\bar{E}_l$). In IISP, the plasma carriers, viz. electrons and charged colloids contribute to the Brillouin susceptibility. In order to avoid the complexities in the formulation of Brillouin susceptibility, distinct formulations have been established for the electrons and the implanted colloids.

2.1 Brillouin susceptibility due to electrons

For electrons, the slow component (n_{se}) of perturbed carrier density, including QEs, may be obtained from equations (9a) and (9b) and using equation (3) as:

$$n_{se}=\frac{-i\beta^2 e n_{0e}Z_e k^3 E_s^*}{\varepsilon\rho m_e(\omega_a^2-k^2v_a^2-2i\Gamma_a\omega_a)}\left[(\delta_1^2-i\nu\omega_a)-\frac{k^2\left|\bar{E}_e\right|^2}{(\delta_2^2+i\nu\omega_s)}\right]^{-1} \quad (10)$$

where $\delta_1^2=(\omega_{pe}^2-\omega_a^2)+k^2V_{Fe}^{'2}$, $\delta_2^2=(\omega_{pe}^2-\omega_s^2)+k^2V_{Fe}^{'2}$,

and $\omega_{pe}=\left(\frac{n_{0e}e^2}{m_e\varepsilon}\right)^{1/2}$ is electron plasma frequency.

The induced current density (J_e) including QEs, may be obtained from the relation:

$$J_e(\omega_s)=-n_{se}^*Z_e e v_{0e}, \quad (11)$$

which yields

$$J_e(\omega_s)=\frac{i\varepsilon e Z_e A k\omega_{pe}^2\left|E_0\right|^2E_s^*}{2m_e\Gamma_a\omega_0\omega_a}\left[(\delta_1^2-i\nu\omega_a)-\frac{k^2\left|\bar{E}_e\right|^2}{(\delta_2^2+i\nu\omega_s)}\right]^{-1} \quad (12)$$

where $A=\kappa^2k^2v_a^2$, $\kappa^2=\frac{\beta^2}{\varepsilon C}$, $\omega_s=\omega_0-\omega_a$, $v_{0e}=\frac{\bar{E}_e}{(\nu-i\omega_0)}$.

In deriving equation (12), the oscillatory electron fluid velocity v_{0e} is obtained from equation (4).

The time integral of the induced current density can be used to express induced polarisation. Thus, the induced polarisation (P_e) due to electrons (at ω_s), including QEs, may be obtained from equation (12) as:

$$P_e(\omega_s)=\frac{\varepsilon e A k Z_e\omega_{pe}^2\left|E_0\right|^2E_s^*}{2m_e\Gamma_a\omega_a\omega_0\omega_s}\left[(\delta_1^2-i\nu\omega_a)-\frac{k^2\left|\bar{E}_e\right|^2}{(\delta_2^2+i\nu\omega_s)}\right]^{-1}=\varepsilon_0\chi_{Be}\left|E_0\right|^2E_s^* \quad (13)$$

From equation (13), the Brillouin susceptibility (χ_{Be}) of IISP due to electrons, including QEs, may be obtained as:

$$\chi_{Be}=\frac{\varepsilon_1 e A k Z_e\omega_{pe}^2}{2m_e\Gamma_a\omega_a\omega_0\omega_s}\left((\delta_1^2-i\nu\omega_a)-\frac{k^2\left|\bar{E}_e\right|^2}{(\delta_2^2+i\nu\omega_s)}\right)^{-1}. \quad (14)$$

2.2 Brillouin susceptibility due to implanted colloids

The colloidal grains have a tendency to cling together and develop a net negative charge due to the high mobility of drifting electrons. For implanted colloids, the slow component (n_{sd}) of perturbed carrier density, including QEs, may be obtained from equations (9a) and (9b) and using equation (3) as:

$$n_{sd}^{*}=\frac{-i\beta^{2}en_{0d}Z_{d}k^{3}E_{s}^{*}}{\varepsilon\rho m_{d}(\omega_{a}^{2}-k^{2}v_{a}^{2}-2i\Gamma_{a}\omega_{s})}\left[(\Delta^{2}-\omega_{a}^{2})-\frac{k^{2}\left|\bar{E}_{d}^{2}\right|}{(\Delta^{2}-\omega_{s}^{2})}\right]^{-1}, \tag{15}$$

where $\Delta^{2}=\omega_{pd}^{2}+k^{2}V_{Fd}^{'2}$, in which

$\omega_{pd}=\left(\frac{(Z_{d})^{2}n_{0d}e^{2}}{m_{d}\varepsilon}\right)^{1/2}$ is dust plasma frequency.

The induced current density (J_{d}) including QEs, may be obtained from the relation:

$$J_{d}(\omega_{s})=-n_{sd}^{*}Z_{d}ev_{0d}, \tag{16}$$

which yields

$$J_{d}(\omega_{s})=\frac{i\varepsilon eZ_{d}Ak\omega_{pd}^{2}\left|E_{0}\right|^{2}E_{s}^{*}}{2m_{d}\Gamma_{a}\omega_{a}\omega_{0}}\left[(\Delta^{2}-\omega_{a}^{2})-\frac{k^{2}\left|\bar{E}_{d}^{2}\right|}{(\Delta^{2}-\omega_{s}^{2})}\right]^{-1}, \tag{17}$$

where $A=\kappa^{2}k^{2}v_{a}^{2}$, $\kappa^{2}=\frac{\beta^{2}}{\varepsilon C}$, $\omega_{s}=\omega_{0}-\omega_{a}$, and $v_{0d}=\frac{\bar{E}_{d}}{(-i\omega_{0})}$.

The induced polarisation (P_{d}) due to implanted colloids (at ω_{s}), including QEs, may be obtained as:

$$\begin{aligned}P_{d}(\omega_{s})&=\frac{\varepsilon eAkZ_{d}\omega_{pd}^{2}\left|E_{0}\right|^{2}E_{s}^{*}}{2m_{d}\Gamma_{a}\omega_{a}\omega_{0}\omega_{s}}\left((\Delta^{2}-\omega_{a}^{2})-\frac{k^{2}\left|\bar{E}_{d}^{2}\right|}{(\Delta^{2}-\omega_{s}^{2})}\right)^{-1}.\\&=\varepsilon_{0}\chi_{Bd}\left|E_{0}\right|^{2}E_{s}^{*}.\end{aligned} \tag{18}$$

The Brillouin susceptibility (χ_{Bd}) of IISP due to implanted colloids, including QEs, may be obtained as:

$$\chi_{Bd}=\frac{\varepsilon_{1}eAkZ_{d}\omega_{pd}^{2}}{2m_{d}\Gamma_{a}\omega_{a}\omega_{0}\omega_{s}}\left((\Delta^{2}-\omega_{a}^{2})-\frac{k^{2}\left|\bar{E}_{d}^{2}\right|}{(\Delta^{2}-\omega_{s}^{2})}\right)^{-1}. \tag{19}$$

2.3 Effective Brillouin susceptibility of IISP

The effective Brillouin susceptibility ($\chi_{B}^{(e)}$) of IISP, including QEs, is the sum of Brillouin susceptibilities due to electrons (χ_{Be}) and due to implanted colloids (χ_{Bd}). Addition of equations (14) and (19) yields:

$$\begin{aligned}\chi_{B}^{(e)}&=\chi_{Be}+\chi_{Bd}\\&=\frac{\varepsilon_{1}eAk}{2\Gamma_{a}\omega_{a}\omega_{0}\omega_{s}}\times\left[\frac{Z_{e}\omega_{pe}^{2}}{m_{e}}\left((\delta_{1}^{2}-i\nu\omega_{a})-\frac{k^{2}\left|\bar{E}_{e}\right|^{2}}{(\delta_{2}^{2}+i\nu\omega_{s})}\right)^{-1}+\frac{Z_{d}\omega_{pd}^{2}}{m_{d}}\left((\Delta^{2}-\omega_{a}^{2})-\frac{k^{2}\left|\bar{E}_{d}^{2}\right|}{(\Delta^{2}-\omega_{s}^{2})}\right)^{-1}\right].\end{aligned} \tag{20}$$

It can be inferred from equation (20) that both electrons and implanted charged colloids contribute to the formulation of $\chi_{B}^{(e)}$. The expressions for $\chi_{B}^{(e)}$ of IISP, excluding QEs, can be obtained by putting $V_{Fe}^{'}=0$ (in δ_{1}, δ_{2} and Δ) in equation (20).

2.4 Threshold pump intensity for OPCM

In order to determine the threshold pump intensity and the reflectivity of OPCM, including QEs, in IISPs, the well known Maxwell's equations are employed to describe induced polarization and polarization effects. The generalised electromagnetic wave equation can be expressed as [44]:

$$\frac{\partial^2 E}{\partial x^2}-\frac{1}{c^2}\frac{\partial^2 E}{\partial t^2}=\mu_0\frac{\partial^2 P_{ind}}{\partial t^2}, \tag{21}$$

where μ_0 and c are the permittivity of free space and velocity of light in the medium, respectively. P_{ind} represents the total induced polarization, which is the sum of linear and nonlinear polarization of the crystal. Using Equation (21), the steady-state coupled wave equations for the pump and the backward Stokes mode in one dimension, including QEs, are obtained as [24]:

$$\frac{\partial E_0}{\partial x}-\left(\frac{i}{2k_0}\right)\frac{\partial^2 E_0}{\partial x^2}+i\alpha_{Ir0}E_0-\alpha_{I0}E_0=-\frac{i\omega_0^2}{2k_0c^2}\chi_{B,0}^{(e)}\left|E_s\right|^2E_0 \tag{22a}$$

and

$$\frac{\partial E_s}{\partial x}-\left(\frac{i}{2k_s}\right)\frac{\partial^2 E_s}{\partial x^2}-i\alpha_{Irs}E_s+\alpha_{Is}E_s=\frac{i\omega_s^2}{2k_sc^2}\chi_{B,s}^{(e)}\left|E_0\right|^2E_s. \tag{22b}$$

Here $\alpha_{I0}=\frac{\omega_0}{2c}\left[\chi_{I0}^{(1)}+\chi_{B,I0}^{(e)}\left|E_s\right|^2\right]$ represents the intensity dependent absorption coefficients of IISPs at pump frequency ω_0,

$\alpha_{Is}=\frac{\omega_s}{2c}\left[\chi_{Is}^{(1)}+\chi_{B,Is}^{(e)}\left|E_s\right|^2\right]$ represents the intensity dependent absorption coefficients of IISPs at Stokes mode frequency ω_s,

$\alpha_{Ir0}=\frac{\omega_0}{2c}\left[\chi_{r0}^{(1)}+\chi_{B,r0}^{(e)}\left|E_s\right|^2\right]$ represents the contribution arising due to dispersive property of IISPs at pump frequency ω_0,

$\alpha_{Irs}=\frac{\omega_s}{2c}\left[\chi_{rs}^{(1)}+\chi_{B,rs}^{(e)}\left|E_0\right|^2\right]$ represents the contribution arising due to dispersive property of IISPs at Stokes mode frequency ω_s,

$\chi_{B,r0}^{(e)}$ is the real part of $\chi_B^{(e)}$ associated with pump frequency ω_0, and

$\chi_{B,rs}^{(e)}$ is the real part of $\chi_B^{(e)}$ associated with Stokes mode frequency ω_s.

In the present analytical investigation of QEs on OPC-SBS, the phase matching conditions which are to be satisfied for interacting waves are: $\hbar\omega_0=\hbar\omega_s+\hbar\omega_a$ and $\hbar\vec{k}_0=-\hbar\vec{k}_s+\hbar\vec{k}_a$; known as energy and momentum conservation relations, respectively. For OPCM, under the condition $\vec{k}_0=-\vec{k}_s$, one should have $\vec{k}_a=2\vec{k}_0$. In the forthcoming analysis, let us assume $\left|\vec{k}_0\right|=\left|\vec{k}_s\right|=k$. Consequently, $\left|\vec{k}_a\right|=2k$ and for low acoustic phonon mode frequency ($\omega_0\gg\omega_a$), one may consider $\omega_0\cong\omega_s=\omega$ (say). Under these assumptions, one can take $\alpha_{I0}=\alpha_{Is}=\alpha_I$ (say) and $\chi_{B,0}^{(e)}\cong\chi_{B,s}^{(e)}=-i\left|\chi_B^{(e)}\right|$ (say), with $\chi_B^{(e)}$ being the complex effective Brillouin susceptibility (including QEs).

Following the single-mode analysis, the phase conjugate Stokes mode electric field is related to the pump wave electric field via relation [45]:

$$E_s(r_\perp,x)=R(x)E_0^*(r_\perp,x), \tag{23}$$

where $R(x)$ is a conjugacy factor and $\left|R(x)\right|^2$ is known as reflectivity of OPCM.

Using Equations (22a) and (22b), the equations for electric field associated with pump wave and Stokes mode, including QEs, can be obtained as [24]:

$$\frac{\partial E_0}{\partial x}+i\alpha_{Ir}E_0-\alpha_IE_0=-\frac{i\omega^2}{2kc^2}\chi_B^{(e)}\left|E_s\right|^2E_0 \tag{24a}$$

and

$$\frac{\partial E_s}{\partial x}-i\alpha_{Ir}E_s+\alpha_IE_s=\frac{i\omega^2}{2kc^2}\chi_B^{(e)}\left|E_0\right|^2E_s \tag{24b}$$

Since $\left|E_s\right|^2$ is a generated field and $E_s(x=0)\sim10^{-13}E_0$ [1], one may safely assume $\alpha_I\gg\frac{\omega^2\chi_B^{(e)}\left|E_s(0)\right|^2}{2kc^2}$. Therefore

$$E_0(x)=\left[E_0(L)\exp\{-\alpha_I(L-x)\}\right]\exp\{i\alpha_{Ir}(L-x)\}, \tag{25}$$

where $E_0(L)$ is the pump wave electric field at $x=L$ (entrance window) of Brillouin medium. Equation (25) manifests the dependence of pump amplitude as well as the nature of phase variation of electric field on path length of semiconductor crystal x. Using equations (24b) and (25), the electric field associated with back-scattered Stokes mode, including QEs, can be obtained as [24]:

$$E_s(x) = E_s(0).\exp\left[\frac{\kappa\{1-\exp(2\alpha_I x)\}}{2\alpha_I} - \alpha_I x\right].\exp\{i\alpha_{Ir} x\}, \tag{26a}$$

where

$$\kappa = \frac{\omega^2 \chi_B^{(e)}}{2kc^2}\left|E_0(L)\right|^2 \exp(-2\alpha_I L)\,. \tag{26b}$$

$E_s(0)$ is pump wave electric field at exit window ($x = 0$) of Brillouin medium and is defined as spontaneous noise field. Equation (26a) can be expressed as:

$$E_s(x) = E_s^{'}(0)\left[\cos(\alpha_{Ir} L) + i\sin(\alpha_{Ir} L)\right].\exp\{-i\alpha_{Ir}(L-x)\} \tag{27a}$$

where

$$E_s^{'}(0) = E_s(0).\exp\left[\frac{\kappa\{1-\exp(2\alpha_I x)\}}{2\alpha_I} - \alpha_I x\right]. \tag{27b}$$

The gain constant associated with the back-scattered Brillouin mode $E_s(x)$, including QEs, is given by

$$\exp\left[\frac{\kappa\{1-\exp(2\alpha_I x)\}}{2\alpha_I} - \alpha_I x\right]. \tag{28a}$$

In order to obtain finite gain of back-scattered Stokes mode, the following condition should be satisfied [24]:

$$\frac{\kappa\{1-\exp(2\alpha_I x)\}}{2\alpha_I} - \alpha_I x < 0\,. \tag{28b}$$

If a semiconductor waveguide of thickness mm is illuminated by an off-resonant laser with photon energy smaller than the band-gap energy of the crystal, this inequality can be resolved in a straightforward manner. On the basis of this premise, one may take $2\alpha_I x < 1$. Consequently, the threshold value of pump intensity for OPCM, including QEs, is given by

$$I_{0T} = \frac{\eta\varepsilon_0 c^3 \alpha k}{\omega^2 \chi_B^{(e)}},$$

$$= \frac{2\eta\varepsilon_0 c^3 \alpha k \Gamma_a \omega_a}{\varepsilon_1 eAk}\left[\frac{Z_e \omega_{pe}^2}{m_e}\left((\delta_1^2 - i\nu\omega_a) - \frac{k^2\left|\bar{E}_e\right|^2}{(\delta_2^2 + i\nu\omega_s)}\right)^{-1} + \frac{Z_d \omega_{pd}^2}{m_d}\left((\Delta^2 - \omega_a^2) - \frac{k^2\left|\bar{E}_d^2\right|}{(\Delta^2 - \omega_s^2)}\right)^{-1}\right]^{-1} \tag{29}$$

where η is the background refractive index, α is the background absorption coefficient of semiconductor crystal, and $I_{0T} = \frac{1}{2}\eta\varepsilon_0 c\left|E_{0T}\right|^2$.

The expression for I_{0T}, excluding QEs, can be obtained by putting $V_{Fe}^{'} = 0$ (in δ_2) in equation (29). I_{0T} is significantly affected by the wave number magnitude k, electron concentration n_{0e} (via ω_{pe} in δ_2), and quantum correction term (via δ_1, δ_2 and Δ).

2.5 Reflectivity of OPCM

Using equations (25) and (27), the reflectivity of OPCM (at $x = L$), including QEs, is given by

$$\left|R(L)\right|^2 = \left(\frac{\left|E_s(0)\right|}{\left|E_0(L)\right|}\right)^2 \exp\left[2\left\{\alpha(L-2x) - \frac{\kappa}{2\alpha}\left\{e^{2\alpha x} - 1\right\}\right\}\right]. \tag{30}$$

The expression for $\left|R(L)\right|^2$, excluding QEs, can be obtained by putting $V_{Fe}^{'} = 0$ (in δ_2) in equation (30). For small laser-semiconductor interaction length, $2\alpha x < 1$. Consequently, equation (30) reduces to:

$$|R(L)|^2 = \left[\frac{|E_s(0)|}{|E_0(L)|}\right]^2 \exp\left[2\{\alpha(L-2x)+\kappa x\}\right]$$

$$= \left[\frac{|E_s(0)|}{|E_0(L)|}\right]^2 \exp\left[2\left\{\alpha(L-2x)+\frac{\omega^2\chi_B^{(e)}x}{2kc^2}|E_0(L)|^2\exp(-2\alpha_I L)\right\}\right]. \quad (31)$$

In equation (31), the generated spontaneous noise field at the entrance window $E_s(0) \approx 10^{-13}|E_0(L)|^2$ [1]. Hence, in order to obtain high reflectivity of OPCM in IISPs, one should have $2\{\alpha(L-2x)+\kappa x\} \approx 30$. This enables one to have a gain $\sim e^{30}$ and reflectivity of OPCM, including QEs, $|R(x)|^2 \approx 1$.

For a back-scattered OPCM, it is simple to obtain from equation (31) that at $x = L$, for IISP of length L, $(\kappa-\alpha)L = 15$ and $|R(x=L)|^2 \approx 1$. This finding is in good agreement with the experimental findings of Zeldovich et al. [1]. Using equations (28) and (29), it is clear that at pump intensity $I_0(L) > I_{0T}$, reflectivity of OPCM, including QEs $|R(L)|^2 \approx 1$ can be obtained in IISPs with sample length $L \approx$ millimeter.

Equation (29) manifests that the threshold intensity I_{0T} for OPCM may be brought lower by assuming a laser-IISP interaction system having large Brillouin susceptibility $\chi_B^{(e)}$. Moreover, the reflectivity of OPCM $|R(L)|^2$ depends on $\chi_B^{(e)}$ (via κ) [Equation (31)], therefore an enhancement in $|R(L)|^2$ is possible if one obtains larger $\chi_B^{(e)}$ in IISP (Brillouin) medium.

3. Results and discussion

The study presented in the preceding section clearly reveals that one may observe OPC-SBS in IISPs by employing the QHD model for the electron dynamics. To have a numerical appreciation of the results obtained in the analysis, let us consider n-InSb crystal as a Brillouin active medium with L = 5 mm at temperature 77 K irradiated by 10.6 μm pulsed CO_2 laser. The stimulation for the selection of n-InSb for OPC-SBS analysis stems from the extensive technological applications it has already found for itself in modern optoelectronics [46, 47]. The relevant parameters of InSb are given in Table 1 [48]. The values of $\chi_B^{(e)}$, I_{0T}, and $|R(L)|^2$ are determined under two categories, viz. excluding QEs and including QEs, and are shown in Table 2. The determined values of $\chi_B^{(e)}$ due to electrons and due to implanted colloids are well in agreement with available literature using CHD model [49] and QHD model [39].

Table 1: Material parameters for n-InSb/CO_2 laser system.

Parameter	Symbol	Units	Value
Dielectric constant	ε_1	---	17.8
Fermi temperature	T_F	K	77
Electron's rest mass	m_0	kg	9.1×10^{-31}
Electron's effective mass	M	($\times m_0$)	0.014
Colloids mass	m_d	kg	1.67×10^{-27}
Crystal mass density	ρ	kg m^{-3}	5.8×10^{3}
Acoustic damping parameter	Γ_a	s^{-1}	2×10^{10}
Piezoelectric coefficient	β	Cm^{-2}	0.054
Electron collision frequency	ν_e	s^{-1}	3.5×10^{11}
Pump wave frequency	ω_0	s^{-1}	1.78×10^{14}
Acoustic wave frequency	ω_a	s^{-1}	2×10^{11}
Acoustic wave velocity	v_a	ms^{-1}	4×10^{3}

Table 2: Calculated values of I_{0T} and $|R(L)|^2$ around resonances $\omega_{pe}^2 \sim \omega_a^2$ and $\omega_{pe}^2 \sim \omega_s^2$ (when QEs are excluded), and $\omega_{pe}^2 \sim \omega_a^2 + k^2V_{Fe}^{'2}$ and $\omega_{pe}^2 \sim \omega_s^2 + k^2V_{Fe}^{'2}$ (when QEs are included).

Parameter		Units	Calculated values			
			(Excluding QEs)		(Including QEs)	
			$\omega_{pe}^2 \sim \omega_a^2$	$\omega_{pe}^2 \sim \omega_s^2$	$\omega_{pe}^2 \sim \omega_a^2 + k^2V_{Fe}^{'2}$	$\omega_{pe}^2 \sim \omega_s^2 + k^2V_{Fe}^{'2}$
Threshold intensity I_{0T}	for electrons	Wm^{-2}	1.8×10^{10}	7.8×10^{9}	1.6×10^{9}	2.2×10^{8}
	for colloids	Wm^{-2}	3.3×10^{10}	6.5×10^{9}	1.9×10^{9}	3.5×10^{8}
Reflectivity of OPCM $|R(L)|^2$	for electrons	%	0.1	2	11	90
	for colloids	%	0.5	2	13	98

We observed that the plasma carrier concentration significantly affect the effective Brillouin susceptibility and hence the threshold pump intensity as well as the reflectivity of OPCM for both the cases, viz. (i) excluding QEs (when $\omega_{pe}^2 \sim \omega_s^2$), and (ii) including QEs (when $\omega_{pe}^2 \sim \omega_s^2 + k^2 V_{Fe}^{'2}$). Thus, in this case, the following ratios are obtained: $(I_{0T})_{QE} / I_{0T} = 2.8\times10^{-2}$ and $(|R(L)|^2)_{QE} / |R(L)|^2 = 45$.

Similarly, the implanted colloid concentration also affects the effective Brillouin susceptibility and hence the threshold pump intensity as well as the reflectivity of OPCM for both the cases, viz. (i) excluding QEs (when $\omega_{pe}^2 \sim \omega_s^2$), and (ii) including QEs (when $\omega_{pe}^2 \sim \omega_s^2 + k^2 V_{Fe}^{'2}$). Thus, in this case, the following ratios are obtained: $(I_{0T})_{QE} / I_{0T} = 5.3\times10^{-2}$ and $(|R(L)|^2)_{QE} / |R(L)|^2 = 49$.

These illustrate that the inclusion of QEs significantly reduces the threshold intensity and enhances the reflectivity of OPCM in IISPs.

3.1 Threshold characteristics of OPCM

Equation (29), which describes the relationship between the threshold pump intensity (I_{0T}) and other factors, such as wave number magnitude (k), electron concentration (n_{0e}), and implanted colloid concentration (n_{0d}) can be used for understanding the nature of the dependence. Figures 1, 2 and 3 provide a plot of the results.

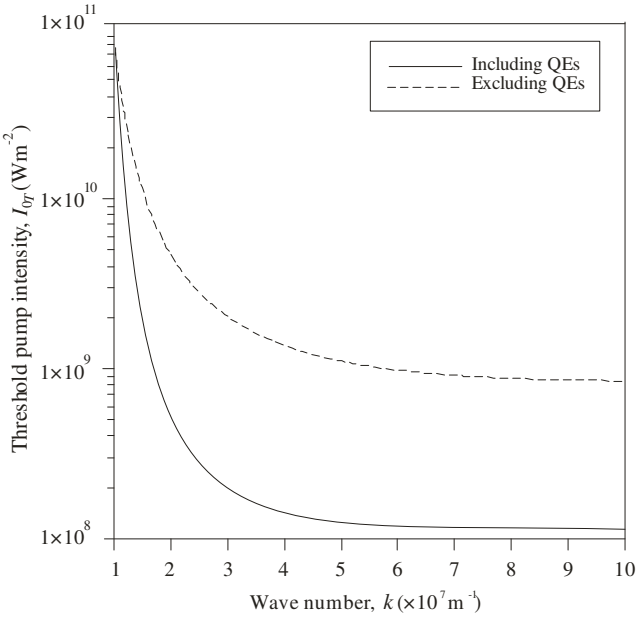

Figure 1: Variation of threshold intensity I_{0T} with wave number magnitude k for the cases: (i) excluding QEs, and (ii) including QEs.

Figure 1 depicts the relationship between threshold pump intensity I_{0T} and wave number magnitude k in the two cases: (i) excluding QEs), and (ii) including QEs. In both instances, we found that the nature of the curves is essentially the same; the difference is that when QEs are included, I_{0T} is significantly lower than when they are excluded. The curves corresponding to both situations coincide for smaller magnitudes of wave number (~ 10^7 m^{-1}), but they gradually diverge as wave number increases, showing that QEs on I_{0T} are more evident at greater magnitudes of wave number. The threshold pump amplitude decreases very rapidly with wave number magnitude for $k < 3\times10^7$ m^{-1}, the rate of fall decreases in the regime 3×10^7 m^{-1} $\le k \le 5\times10^7$ m^{-1}, and then becomes nearly independent for $k > 5\times10^7$ m^{-1}. The nature of curves can be understood from equation (29). When QEs are not taken into account ($V_{Fe}^{'} = 0$ and hence $\delta_2 = 0$), $I_{0T} \propto k^{-1}$. However, when QEs are taken into account, the term δ_1^2 containing k gets additionally modified and I_{0T} exhibits the complex dependence on k.

Figure 2 depicts how the threshold pump intensity I_{0T} varies with electron concentration n_{0e} in the two cases: (i) when QEs, and (ii) including QEs.

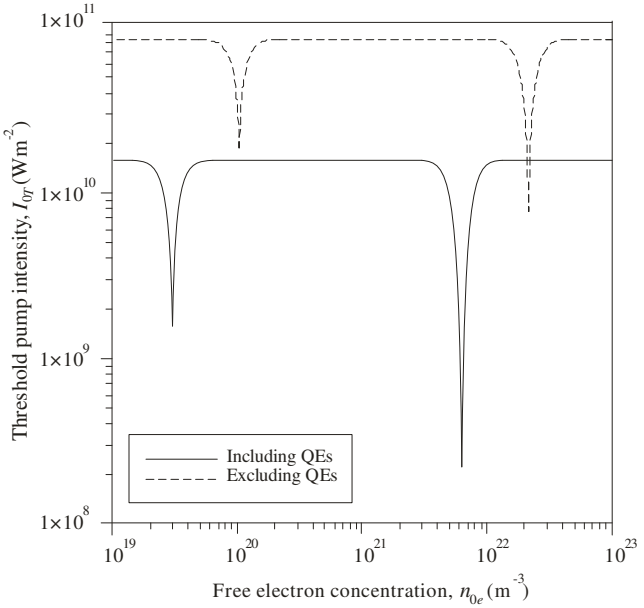

Figure 2: Variation of threshold intensity I_{0T} with electron concentration n_{0e} for the cases: (i) excluding QEs, and (ii) including QEs.

When QEs are not taken into account ($V_{Fe}^{'} = 0$), I_{0T} is comparatively larger, remains independent of n_{0e}, except at $n_{0e} = 1.1\times10^{20}$ and 1.2×10^{22} m^{-3}. At these particular value of n_{0e}, I_{0T} exhibit minimization which are caused by resonances: $\omega_{pe}^2 \sim \omega_a^2$ (via δ_1^2) and $\omega_{pe}^2 \sim \omega_s^2$ (via δ_2^2). When QEs are included ($V_{Fe}^{'} \neq 0$), the plot's features are unaltered with the exception of the shifted peak value of the curve (at $n_{0e} = 2\times10^{19}$ and 6×10^{21} m^{-3}) towards smaller values of electron concentration and I_{0T} has been decreased significantly throughout the plotted regime of n_{0e}. This change occurred due to inclusion of QEs via appearance of the term $k^2 V_{Fe}^{'2}$ in δ_1^2 and δ_2^2. In this case, the behaviour of I_{0T} is caused by resonances: $\omega_{pe}^2 \sim \omega_a^2 + k^2 V_{Fe}^{'2}$ (via δ_1^2) and $\omega_{pe}^2 \sim \omega_s^2 + k^2 V_{Fe}^{'2}$ (via δ_2^2). Thus, around resonances, the threshold intensity reduces by one order of magnitude when QEs are excluded and two orders of magnitude when QEs are included.

It is important to note that the reduction of the threshold pump intensity necessary for OPC-SBS in magnetised semiconductor plasmas was achieved by Singh and Aghamkar [43] by establishing the single resonance $(\omega_s)_m \sim \omega_s\{1-(2\omega_c^2/\omega_p^2)\}\{1-(\omega_c^2/\omega_p^2)\}$; Aghamkar and

Singh [43] by establishing two resonances ($2\omega_c^2 \sim \omega_0^2$ and $\omega_c^2 \sim \omega_0^2$), and Bhan et al. [24] by establishing two resonances ($\omega_c^2 \sim \omega_s^2$ and $\omega_c^2 \sim \omega_0^2$). These studies were carried out by excluding QEs. Moreover, in none of these studies, the shifting of minimization curves was not observed. But in the present study, we obtained the minimization of threshold pump intensity required for OPC-SBS in (un-magnetized) IISPs by setting up only a single resonance in each case, viz. $\omega_{pe}^2 \sim \omega_s^2$ (when QEs are excluded), and $\omega_{pe}^2 \sim \omega_s^2 + k^2 V_{Fe}^{'2}$ (when QEs are included). Also, we observed shifting of minimization curve towards smaller values of electron concentration, with inclusion of QEs.

Figure 3 shows how the threshold pump intensity I_{0T} varies with implanted colloid concentration n_{0d} for the cases: (i) in which QEs are excluded and (ii) in which QEs are included. To draw this behaviour, we consider the contribution of n_{0d} to I_{0T}; the contribution of n_{0e} to I_{0T} is neglected. We consider the wide range of implanted colloid concentration ($10^2\,\mathrm{m}^{-3} < n_{0d} < 10^6\,\mathrm{m}^{-3}$). This clearly shows the substantial reduction of I_{0T}. For clear understanding, the features corresponding to both the cases can be explained separately.

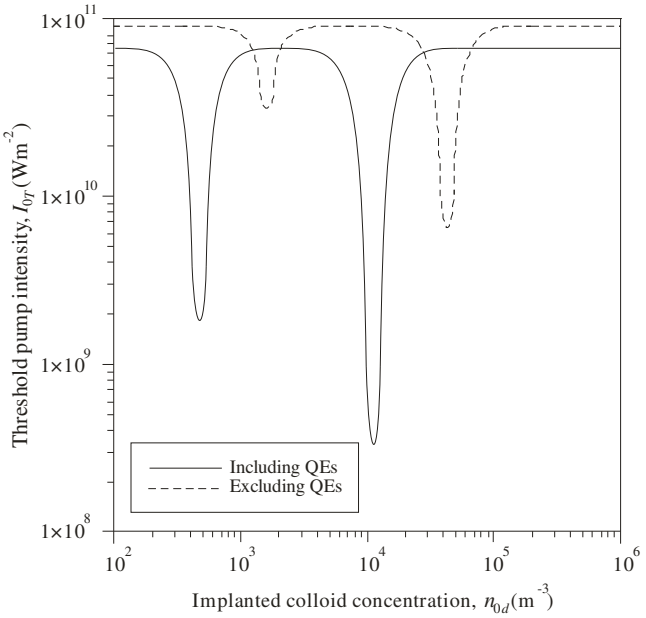

Figure 3: Variation of threshold intensity I_{0T} with implanted colloid concentration n_{0d} for the cases: (i) excluding QEs, and (ii) including QEs.

When QEs are not taken into account ($V_{Fd}^{'} = 0$), I_{0T} is comparatively large (~ 10^{11} Wm^{-2}) and remain unaffected by the implanted colloid concentration for $n_{0d} \le 9\times10^2\,\mathrm{m}^{-3}$. The regime $9\times10^2\,\mathrm{m}^{-3} < n_{0d} \le 3\times10^3\,\mathrm{m}^{-3}$ is quite sensitive to the nature of curve. In this regime, with increasing n_{0d}, I_{0T} starts decreasing sharply, achieving minimum at $n_{0d} = 1.7\times10^3\,\mathrm{m}^{-3}$ and increases sharply achieving its previously higher value at $n_{0d} = 3\times10^3\,\mathrm{m}^{-3}$. For $4\times10^3\,\mathrm{m}^{-3} < n_{0d} \le 1.7\times10^4\,\mathrm{m}^{-3}$, I_{0T} remains unaffected by the implanted colloid concentration. The nature of curve of I_{0T} versus n_{0d} is repeated again in the regime $2.5\times10^4\,\mathrm{m}^{-3} \le n_{0d} \le 8\times10^4\,\mathrm{m}^{-3}$ like the regime $9\times10^2\,\mathrm{m}^{-3} < n_{0d} \le 3\times10^3\,\mathrm{m}^{-3}$. For $n_{0d} > 8\times10^4\,\mathrm{m}^{-3}$, I_{0T} being comparatively larger and remain unaffected by the implanted colloid concentration. The behaviour of I_{0T} in the domain $9\times10^2\,\mathrm{m}^{-3} < n_{0d} \le 3\times10^3\,\mathrm{m}^{-3}$ is caused by resonance between frequencies of dust plasma wave and acoustic wave, i.e. $\omega_{pd}^2 \sim \omega_a^2$ (via Δ^2) while the behaviour of I_{0T} in the domain $2.5\times10^4\,\mathrm{m}^{-3} \le n_{0d} \le 8\times10^4\,\mathrm{m}^{-3}$ is caused by resonance between the frequencies of dust plasma wave and OPCM, i.e. $\omega_{pe}^2 \sim \omega_s^2$ (via Δ^2).

When QEs are taken into account ($V_{Fd}^{'} \neq 0$), the entire spectrum has been shifted towards smaller values of colloid concentration and the minimization curves of I_{0T} have been minimized significantly. The minimization of I_{0T} previously occurred at $n_{0d} = 1.7\times10^3$, and $4\times10^3\,\mathrm{m}^{-3}$, have now been shifted to $n_{0d} = 5\times10^2$, and $1.1\times10^4\,\mathrm{m}^{-3}$, respectively. This change occurred due to inclusion of QEs via appearance of the term $k^2V_{Fd}^{'2}$ in Δ^2. In this case, the minimization of I_{0T} at $n_{0d} = 1.7\times10^3\,\mathrm{m}^{-3}$ is caused by resonance between frequencies of dust plasma wave and acoustic wave modified by the quantum correction term, i.e. $\omega_{pd}^2 \sim \omega_a^2 + k^2V_{Fd}^{'2}$ and the minimization of I_{0T} at $n_{0d} = 4\times10^3\,\mathrm{m}^{-3}$ is caused by resonance between frequencies of dust plasma wave and OPCM modified by the quantum correction term, i.e. $\omega_{pd}^2 \sim \omega_s^2 + k^2V_{Fd}^{'2}$. In IISPs, these resonances can be set up by proper selection of implanted colloid concentration. Around resonances I_{0T} can be reduced by one to two orders of magnitude.

3.2 Reflectivity characteristics of OPCM

Equation (30) can be used to study the nature of the dependency of reflectivity ($|R(L)|^2$) of OPCM on several factors, including wave number magnitude (k), electron concentration (n_{0e}), implanted colloid concentration (n_{0d}), and pump intensity (I_0). Figures 4, 5, 6 and 7 display the results.

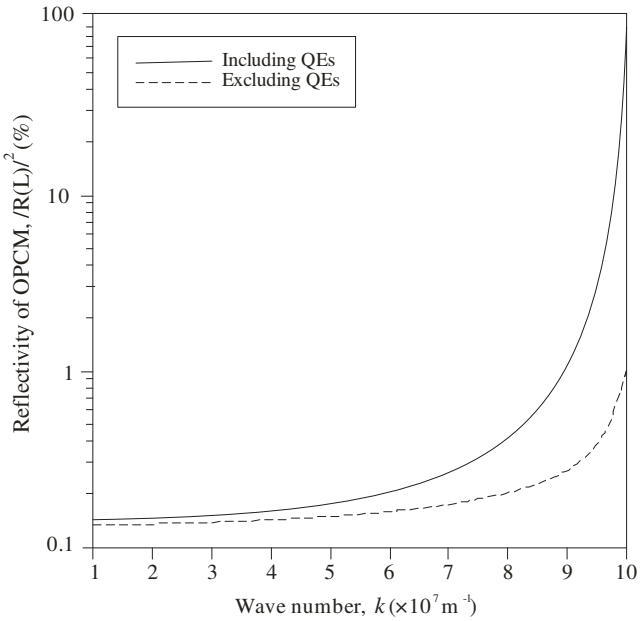

Figure 4: Variation of reflectivity $|R(L)|^2$ of OPCM with wave number magnitude k for the cases: (i) excluding QEs, and (ii) including QEs.

Figure 4 depicts the relationship between the reflectivity $|R(L)|^2$ of OPCM and wave number magnitude k in the two cases: (i) excluding QEs), and (ii) including QEs. In both

cases, we found that the nature of the curves is essentially the same; the difference is that when QEs are included, $|R(L)|^2$ is significantly greater than when they are excluded. The curves corresponding to both cases are extremely close to one another for smaller magnitudes of wave number (~ 10^7 m^{-1}), but they gradually diverge as wave number increases, showing that QEs on $|R(L)|^2$ are more pronounced at greater magnitudes of wave number. The reflectivity of OPCM exhibits a linear variation with wave number magnitude for $k \le 5\times10^7\,m^{-1}$ and then exhibit rapid increment for $k > 5\times10^7\,m^{-1}$. The nature of curves can be understood from equation (30). When QEs are not taken into account ($V_{Fe}^{'}=0$ and hence $\delta_2=0$), $|R(L)|^2 \propto k$. However, when QEs are taken into account, the terms δ_1^2 and δ_2^2 containing k gets additionally modified and $|R(L)|^2$ exhibits the parabolic dependence on k.

Figure 5 depicts the relationship between reflectivity $|R(L)|^2$ of OPCM and electron concentration n_{0e} in the two cases: (i) excluding QEs), and (ii) including QEs.

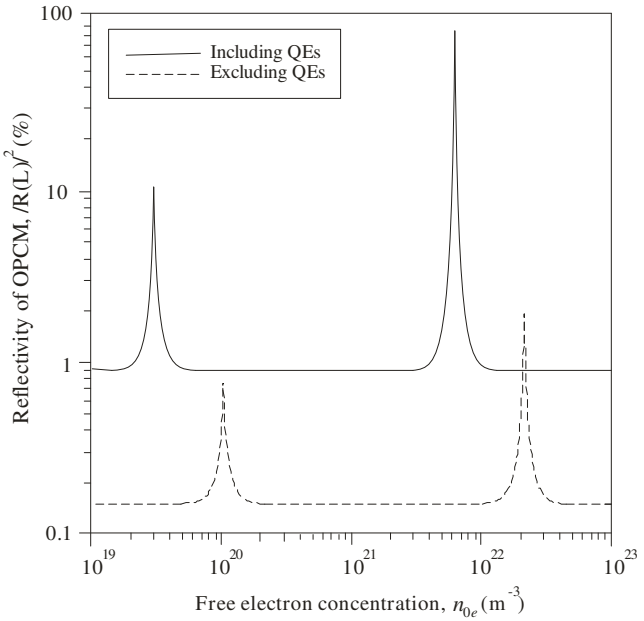

Figure 5: Variation of reflectivity $|R(L)|^2$ of OPCM with electron concentration n_{0e} for the cases: (i) excluding QEs, and (ii) including QEs.

When QEs are not taken into account ($V_{Fe}^{'}=0$), $|R(L)|^2$ is comparatively smaller, remains independent of n_{0e}, except at $n_{0e}=1.1\times10^{20}$ and 1.2×10^{22} m^{-3}. At these particular value of n_{0e}, $|R(L)|^2$ exhibit sharp peaks which are caused by resonances: $\omega_{pe}^2 \sim \omega_a^2$ (via δ_1^2) and $\omega_{pe}^2 \sim \omega_s^2$ (via δ_2^2). When QEs are included ($V_{Fe}^{'}\neq0$), the plot's features are unaltered with the exception of the shifted peak value of the curve (at $n_{0e}=2\times10^{19}$ and 6×10^{21} m^{-3}) towards smaller values of electron concentration and $|R(L)|^2$ has been increased significantly throughout the plotted regime of n_{0e}. This change occurred due to inclusion of QEs via appearance of the term $k^2V_{Fe}^{'2}$ in δ_1^2 and δ_2^2. In this case, the behaviour of $|R(L)|^2$ is caused by resonances: $\omega_{pe}^2 \sim \omega_a^2 + k^2V_{Fe}^{'2}$ (via δ_1^2) and $\omega_{pe}^2 \sim \omega_s^2 + k^2V_{Fe}^{'2}$ (via δ_2^2). Thus, around resonances, the reflectivity of OPCM increases by one order of magnitude when QEs are excluded and two orders of magnitude when QEs are included.

It is important to note that an enhancement of reflectivity of OPCM in magnetised semiconductor plasmas was achieved by Singh and Aghamkar [9] by establishing the single resonance $(\omega_s)_m \sim \omega_s\{1-(2\omega_c^2/\omega_p^2)\}\{1-(\omega_c^2/\omega_p^2)\}$; Aghamkar and Singh [22] by establishing two resonances ($2\omega_c^2 \sim \omega_0^2$ and $\omega_c^2 \sim \omega_0^2$), and Bhan et al. [24] by establishing two resonances ($\omega_c^2 \sim \omega_s^2$ and $\omega_c^2 \sim \omega_0^2$). These studies were carried out by excluding QEs. Moreover, in none of these studies, the shifting of peak of the curves was not observed. But in the present study, we obtained the substantial enhancement of reflectivity of OPCM in (un-magnetized) IISPs by setting up only a single resonance in each case, viz. $\omega_{pe}^2 \sim \omega_s^2$ (when QEs are excluded), and $\omega_{pe}^2 \sim \omega_s^2 + k^2V_{Fe}^{'2}$ (when QEs are included). Also, we observed the shifting of peak of curves towards smaller values of electron concentration, with inclusion of QEs. This shifting may be advantageous in the development of widely tunable Brillouin lasers.

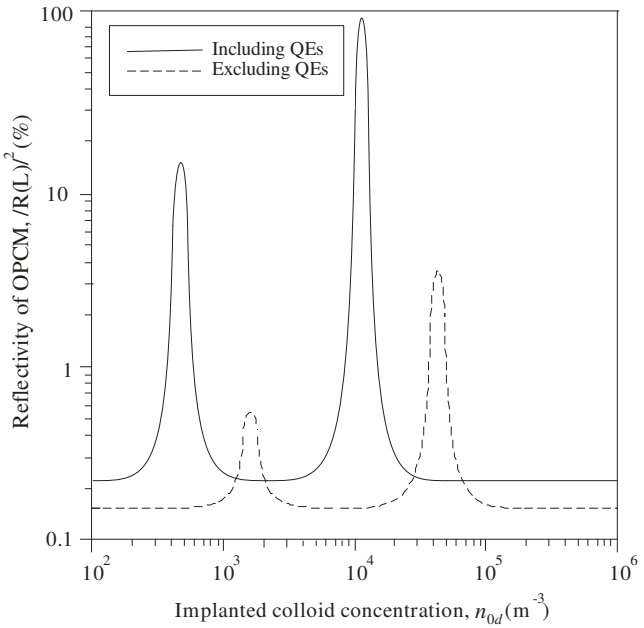

Figure 6: Variation of reflectivity $|R(L)|^2$ of OPCM with implanted colloid concentration n_{0d} for the cases: (i) excluding QEs, and (ii) including QEs.

Figure 6 shows how the reflectivity $|R(L)|^2$ of OPCM varies with implanted colloid concentration n_{0d} for the cases: (i) in which QEs are excluded and (ii) in which QEs are included. To draw this behaviour, we consider the contribution of n_{0d} to $|R(L)|^2$; the contribution of n_{0e} to $|R(L)|^2$ is neglected. We consider the wide range of implanted colloid concentration ($10^2\,m^{-3} < n_{0d} < 10^6\,m^{-3}$). This clearly shows the substantial enhancement of $|R(L)|^2$. For clear understanding, the features corresponding to both the cases can be explained separately.

When QEs are not taken into account ($V_{Fd}^{'}=0$), $|R(L)|^2$ is negligibly small (< 1%) and remain unaffected by the implanted colloid concentration for $n_{0d} \le 9\times10^2\,m^{-3}$. The regime $9\times10^2\,m^{-3} < n_{0d} \le 3\times10^3\,m^{-3}$ is quite sensitive to the

nature of curve. In this regime, with increasing n_{0d}, $|R(L)|^2$ starts increasing sharply, achieving peak value at $n_{0d} = 1.7\times10^3\ \mathrm{m}^{-3}$ and decreases sharply achieving its previously smaller value at $n_{0d} = 3\times10^3\ \mathrm{m}^{-3}$. For $4\times10^3\ \mathrm{m}^{-3} < n_{0d} \le 1.7\times10^4\ \mathrm{m}^{-3}$, $|R(L)|^2$ remains unaffected by the implanted colloid concentration. The nature of curve of $|R(L)|^2$ versus n_{0d} is repeated again in the regime $2.5\times10^4\ \mathrm{m}^{-3} \le n_{0d} \le 8\times10^4\ \mathrm{m}^{-3}$ like the regime $9\times10^2\ \mathrm{m}^{-3} < n_{0d} \le 3\times10^3\ \mathrm{m}^{-3}$. For $n_{0d} > 8\times10^4\ \mathrm{m}^{-3}$, $|R(L)|^2$ being comparatively smaller and remain unaffected by the implanted colloid concentration. The behaviour of $|R(L)|^2$ in the domain $9\times10^2\ \mathrm{m}^{-3} < n_{0d} \le 3\times10^3\ \mathrm{m}^{-3}$ is caused by resonance between frequencies of dust plasma wave and acoustic wave, i.e. $\omega_{pd}^2 \sim \omega_a^2$ (via Δ^2) while the behaviour of $|R(L)|^2$ in the domain $2.5\times10^4\ \mathrm{m}^{-3} \le n_{0d} \le 8\times10^4\ \mathrm{m}^{-3}$ is caused by resonance between the frequencies of dust plasma wave and OPCM, i.e. $\omega_{pe}^2 \sim \omega_s^2$ (via Δ^2).

When QEs are taken into account ($V_{Fd}^{'} \neq 0$), the entire spectrum has been shifted towards smaller values of colloid concentration and the peak of curves of $|R(L)|^2$ have been enhanced significantly. The enhancement of $|R(L)|^2$ previously occurred at $n_{0d} = 1.7\times10^3$, and $4\times10^3\ \mathrm{m}^{-3}$, have now been shifted to $n_{0d} = 5\times10^2$, and $1.1\times10^4\ \mathrm{m}^{-3}$, respectively. This change occurred due to inclusion of QEs via appearance of the term $k^2V_{Fd}^{'2}$ in Δ^2. In this case, the enhancement of $|R(L)|^2$ at $n_{0d} = 1.7\times10^3\ \mathrm{m}^{-3}$ is caused by resonance: $\omega_{pd}^2 \sim \omega_a^2 + k^2V_{Fd}^{'2}$ and the enhancement of $|R(L)|^2$ at $n_{0d} = 4\times10^3\ \mathrm{m}^{-3}$ is caused by resonance: $\omega_{pd}^2 \sim \omega_s^2 + k^2V_{Fd}^{'2}$. In IISPs, these resonances can be set up by proper selection of implanted colloid concentration. Around resonances $|R(L)|^2$ can be enhanced by one to two orders of magnitude and even $|R(L)|^2 \cong 100\%$.

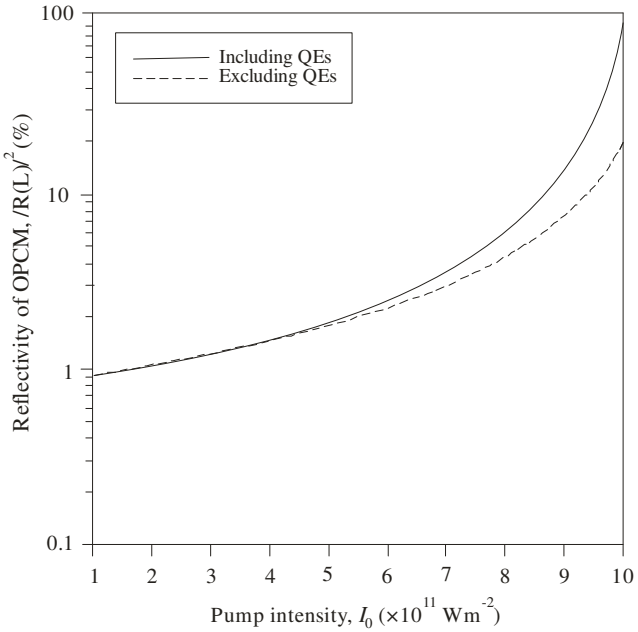

Figure 7: Variation of reflectivity $|R(L)|^2$ of OPCM with pump field amplitude E_0 for the cases: (i) excluding QEs, and (ii) including QEs.

Figure 7 shows how the reflectivity $|R(L)|^2$ of OPCM varies with pump intensity I_0 for the cases: (i) in which QEs are excluded and (ii) in which QEs are included. We noticed that $|R(L)|^2$ exhibits curves of identical shape in both cases across the plotted range of I_0. Both when QEs are excluded and when they are included, the curve has a parabola shape. When QEs are negligible for smaller values of I_0 ($\le 4\times10^{11}$ Wm^{-2}), the curves corresponding to both cases exactly overlap. The curves corresponding to both cases, however, begin to diverge with increasing I_0 ($> 4\times10^{11}$ Wm^{-2}), which is the limit at which QEs become significant. This deviation of $|R(L)|^2$ curves at large pump intensities highlights the need to include QEs in OPC-SBS phenomenon.

4. Conclusions

In this paper, QEs on threshold and reflectivity characteristics of OPCM in IISPs are studied using QHD model. Both, the threshold and reflectivity characteristics of OPCM are strongly dependent on the electron as well as the implanted colloid concentration. The numerical analysis is performed for n-InSb/CO_2 laser system for two different cases, viz. excluding QEs and including QEs. In both the cases, the analysis offers two achievable resonances ($\omega_{pe}^2 \sim \omega_a^2$ and $\omega_{pe}^2 \sim \omega_s^2$, when QEs are excluded, and $\omega_{pe}^2 \sim \omega_a^2 + k^2V_{Fe}^{'2}$ and $\omega_{pe}^2 \sim \omega_s^2 + k^2V_{Fe}^{'2}$, when QEs are included), at which the minimization of threshold intensity and enhancement of reflectivity of OPCM are obtained. The inclusion of QEs in the analysis shifts the entire spectrum towards smaller values of electrons (colloids) carrier concentration. In addition, the reflectivity characteristics of OPCM are insignificant for smaller pump intensities ($\le 4\times10^{11}$ Wm^{-2}) and pronounced at higher pump intensities ($> 4\times10^{11}$ Vm^{-1}). As a result, the investigation improves our understanding of OPC-SBS processes in electron- and colloidal-based IISPs and establishes the suitability of the selected sample for the production of effective optical phase conjugate mirrors.

Acknowledgements

The author is thankful to Dr. Manjeet Singh, Assistant Professor, Department of Physics, Government College, Matanhail (Jhajjar) India for many useful suggestions to carry out this work.

Authors' contributions

The author read and approved the final manuscript.

Conflicts of interest

The author declares no conflict of interest.

Funding

This research received no external funding.

Data availability

No new data were created.

References

[1] B. Ya. Zel'dovich, V.I. Popovichev, V.V. Ragul'skii, F.S. Faizullov, Connection between the wave fronts of the reflected and exciting light in stimulated Mandel'shtam – Brillouin scattering, *JETP Lett*. **15** (1972) 109-113.

[2] A. Brignon, J.P. Huignard, *Phase Conjugate Laser Optics*, Wiley, New York (2003).

[3] S. Jackel, I. Moshe, R. Lavi, Comparison of adaptive optics and phase conjugate mirrors for correction of aberrations in double-pass amplifiers, *Appl. Opt*. **42** (2003) 983-989.

[4] X. Liu, A.R. Chraplyvy, P.J. Winzer, R.W. Tkach, S. Chandrasekhar, Phase-conjugated twin waves for communication beyond the Kerr nonlinearity limit, *Nat. Photon.* **7** (2013) 560-568.

[5] E. Mercier, D. Wolfersberger, M. Sciamanna, High frequency chaotic dynamics enabled by optical phase-conjugation, *Sci. Rep*. **6** (2016) 18988-18996.

[6] A.D. Ellis, M.A. Khateeb, M. McCarthy, Impact of optical phase conjugation on the nonlinear Shannon limit, *J. Lightwave Technol*. **35** (2017) 792-798.

[7] G.S. He, Optical phase conjugation: principles, techniques, and applications, *Prog. Quantum Electron*. **26** (2002) 131-191.

[8] S. Ali, W.M. Moslem, P.K. Shukla, I. Kourakis, Fully nonlinear ion-sound waves in a dense Fermi magnetoplasma, *Phys. Lett. A* **366** (2007) 606-610.

[9] M. Singh, P. Aghamkar, Mechanism of phase conjugation via stimulated Brillouin scattering in narrow bandgap semiconductors, *Opt. Commun*. **281** (2008) 1251-1255.

[10] Y.R. Shen, *Principles of Nonlinear Optics*, John Wiley, New York (1984).

[11] G.K.N. Wong, M.J. Damzen, Enhancement of the phase conjugate stimulated Brillouin scattering process using optical feedback, *J. Mod. Opt*. **35** (1988) 483–490.

[12] M.J. Damzen, M.H.R. Hutchinson, W.A. Schroeder, Single frequency phase conjugate laser resonator using stimulated Brillouin scattering, *Opt. Lett*. **12** (1987) 45–47.

[13] B. Ya. Zel'dovich, F. Pilipetsky, V.V. Shkunov, *Principles of Phase Conjugation*, Springer–Verlag, New York (1985).

[14] D. Anderson, M. Karlsson, M. Lisak, A. Sergeev, Modulation instability dynamics in a spatial focusing and temporal defocusing medium, *Phys. Rev. E* **47** (1993) 3617-3622.

[15] K.D. Ridley, A.M. Scott, High reflectivity phase conjugation using Brillouin pre-amplification, *Opt. Lett*. **15** (1990) 777–779.

[16] R.W. Hellwarth, Theory of phase conjugation by stimulated scattering in a waveguide, *J. Opt. Soc. Am*. **68** (1978) 1050-1056.

[17] P. Suni, J. Falk, Theory of phase conjugation by stimulated Brillouin scattering, *J. Opt. Soc. Am. B* **13** (1986) 1681-1691.

[18] R.H. Lehmberg, Numerical study of phase conjugation in stimulated Brillouin scattering from an optical waveguide, *J. Opt. Soc. Am* **73** (1983) 558-566.

[19] A.M. Scott, M.S. Hazell, High efficiency scattering in transient Brillouin enhanced four-wave mixing, *IEEE J. Quantum Electron*. **QE-22** (1986) 1248-1257.

[20] M. Singh, J. Gahlawat, A. Sangwan, N. Singh, M. Singh, *Nonlinear optical susceptibilities of a piezoelectric semiconductor magneto-plasma*, In: Recent Trends in Materials and Devices, V.K. Jain, S. Rattan, A. Verma (Eds.) Springer Proceedings in Physics, Springer, Singapore (2020) Vol. 256, Ch. 20.

[21] E. Garmire, Resonant optical nonlinearities in semiconductors, *IEEE J. Quantum Electron*. **QE-6** (2000) 1094-1110.

[22] P. Aghamkar, M. Singh, Phase conjugation in weakly piezoelectric magnetized semiconductor-plasmas, *J. Mod. Opt*. **55** (2008) 931-945.

[23] M. Singh, A. Sangwan, S. Redhu, High reflectivity phase conjugation in magnetized diffusion driven semiconductors, *Eur. Phys. J. D* **57** (2010) 403-410.

[24] S. Bhan, S.P. Singh, V. Kumar, M. Singh, Low threshold and high reflectivity of optical phase conjugate mode in transversely magnetized semiconductors, *Optik* **184** (2019) 464-472.

[25] J. Kennedy, J. Leveneur, G.V.M. Williams, D.R.G. Mitchell, Fabrication of surface magnetic nanoclusters using low energy ion implantation and electron beam annealing, *Nanotech*. **22** (2011) 115602.

[26] D. Kumar, S. Gupta, T. Jin, R. Nongjai, A. Kandasami, S.N. Piramanayagam, High energy ion implantation induced modification of structural and magnetic properties of masked CoPt magnetic layers, *IEEE Magnet. Lett*. **9** (2017) 4500305.

[27] W.C. Jung, A study on distributions of boron ions implanted by using B and BF_2 dual implantations in silicon, *Trans. Elect. Electron. Mater*. **11** (2010) 120-125.

[28] M. Salimullah, Z. Ehsan, K. Zubia, H.A. Shah, G. Murtaza, Possible colloid crystal formation in a magnetized and inhomogeneous semiconductor-plasma, *J. Appl. Phys*. **102** (2007) 053301.

[29] I. Zeba, C. Uzma, M. Jamil, M. Salimullah, P.K. Shukla, Colloidal crystal formation in a semiconductor quantum plasma, *Phys. Plasmas* **17** (2010) 032105.

[30] S. Ghosh, P. Khare, Effect of density gradient on the acousto-electric wave instability in ion-implanted semiconductor-plasmas, *Acta Physica Polonica A* **109** (2006) 187-197.

[31] N. Yadav, S. Ghosh, P.S. Malviya, Nonlinear parametric interactions in ion-implanted semiconductor-plasmas having strain-dependent dielectric constants, *Chin. Phys. B* **26** (2017) 015203.

[32] S. Ghosh, P. Khare, Acousto-electric wave instability in ion-implanted semiconductor-plasmas, *European Phys. J. D* **35** (2005) 521-526.

[33] S. Ghosh, P. Thakur, Instability of circularly polarized electro-kinetic waves in magnetized ion-implanted semiconductor-plasmas, *European Phys. J. D* **37** (2006) 417-422.

[34] P.K. Shukla, S. Ali, Dust acoustic waves in quantum plasmas, *Phys. Plasmas* **12** (2005) 114502.

[35] F. Haas,. A magnetohydrodynamic model for quantum plasmas, *Phys. Plasmas* **12** (2005) 062117.

[36] D. Singh, B.S. Sharma, M. Singh, Parametric amplification of acoustical phonons in semiconductor magneto-plasmas: quantum effects, *Materials Today: Proc*. **49** (2022) 1383-1389.

[37] D. Singh, B.S. Sharma, M. Singh, Quantum effects on modulational amplification characteristics of semiconductor magneto-plasmas, *Iran. J. Sci. Technol. Trans. Sci*. **46** (2022) 999-1009.

[38] D. Singh, B.S. Sharma, M. Singh, Quantum corrections on threshold and growth rate of modulational amplification in semiconductor magneto-plasmas, *J. Nonlin. Opt. Phys. Mater*. **31** (2022) 235009.

[39] D. Singh, B.S. Sharma, M. Singh, Quantum effects on threshold and Brillouin gain characteristics of semiconductor magneto-plasmas, *J. Opt*. **51** (2022) 969-978.

[40] Pravesh, S. Dahiya, D. Singh, M. Singh, Quantum effects on modulational amplification in ion-implanted semiconductor magnetoplasmas, *Pramana J. Phys*. **97** (2023) 58.

[41] Pravesh, S. Dahiya, N. Singh, M. Singh, Dispersion, threshold and gain characteristics of Brillouin scattered Stokes mode in ion-implanted semiconductor quantum plasmas, *Optik* **293** (2023) 171452.

[42] Renu, Sanjay, M. Singh, Hot carrier effects on Brillouin gain coefficients of magnetoactive doped semiconductors, *J. Opt*. **51** (2022) 386-396.

[43] M. Singh, P. Aghamkar, N. Kishore, P.K. Sen, Nonlinear absorption and refractive index of Brillouin scattered mode in semiconductor-plasmas by an applied magnetic field, *Opt. Laser Tech*. **40** (2008) 215-222.

[44] D.M. Pepper, Nonlinear optical phase conjuction, *Opt. Eng*. **21** (1982) 156-183.

[45] P. Yeh, 2-wave mixing in nonlinear media, *IEEE J. Quantum Electron*. **QE-25** (1989) 484-519.

[46] S. Mokkapati, C. Jagadish, III-V compound SC for optoelectronic devices, *Mat. Today* **12** (2009) 22-32.

[47] Y. Zhang, J. Wu, M. Aagesen, H. Liu, III-V nanowires and nanowire optoelectronic devices, *J. Phys. D: Appl. Phys*. **48** (2015) 463001.

[48] P. Aghamkar, M. Singh, N. Kishore, S. Duhan, P.K. Sen, Steady-state and transient Brillouin gain in magnetoactive narrow band gap semiconductors, *Semicond. Sci. Technol*. **22** (2007) 749-754.

[49] P. Kumari, B.S. Sharma, M. Singh, Hot carrier effects on Brillouin amplification in semiconductor magneto-plasmas, *Ind. J. Phys*. **96** (2022) 3651-3663.